Applied Surface Science 447 (2018) 254–260

Contents lists available at ScienceDirect

Applied Surface Science

journal homepage: www.elsevier.com/locate/apsusc

Full Length Article

DFT study of hydrogen adsorption on Ni/graphene

S. Amaya-Roncancio *, A.A. García Blanco, D.H. Linares, K. Sapag

Instituto de Física Aplicada-CONICET, Dpto. de Física, Universidad Nacional de San Luis, Chacabuco 917, CP: 5700 San Luis Capital, San Luis, Argentina

ARTICLE INFO

Article history:
Received 21 December 2017
Revised 21 March 2018
Accepted 28 March 2018
Available online 29 March 2018

Keywords:
DFT
Hydrogen storage
Ni_{13} cluster
Ni surface
Graphene

ABSTRACT

DFT calculations with the GGA-PBE exchange correlation functional were used to study H_2 adsorption on a Ni(1 1 1) surface, isolated Ni_{13} cluster, and graphene-supported Ni_{13}. In comparison with Ni(1 1 1), hydrogen adsorption shows to be more stable on isolated Ni_{13} and graphene-supported Ni_{13}. In the graphene-supported Ni_{13}, pseudo charge density difference calculations showed accumulation of charge density around the Ni-graphene interfacial region. Dissociative H_2 adsorption on Ni(1 1 1) and isolated Ni_{13} appears to be a non-activated process, whereas an activation barrier is observed on the graphene-supported Ni_{13}. Additionally, the effect of pre-adsorbed hydrogen in H_2 adsorption in the mentioned systems was studied showing that it stabilizes the final state of adsorbed H and decreases the activation barrier.

1. Introduction

Hydrogen is an energy carrier whose application in the generation of electricity using fuel cells is considered a clean technology which could be used for stationary and mobile applications, from vehicular –about 100 kW- to small mobile devices that require a few watts [1–3]. However, the development of efficient and economic hydrogen storage systems is still a major drawback for the development of a hydrogen economy [2].

Several techniques have been studied for the storage of hydrogen: liquefaction, high-pressure cylinders, metal and complex hydrides formation, and adsorption on nanoporous materials [2–4]. The later one has been evaluated on several materials with high specific surface area, and pores of nanometric dimensions (usually < 2 nm). However, the storage capacities obtained at room temperature are still not suitable for the desired volumetric energy density stored [2,3].

The presence of highly dispersed palladium, platinum, or nickel supported on carbon materials has been reported to improve the amount of adsorbed hydrogen at room temperature. Several authors have attributed this phenomenon to a hydrogen spillover mechanism from the metal surface to the support [4–10]. Nevertheless, the exact interaction mechanism between H_2 and supported Ni is still a matter of research due to the complexity of the metal/support interface [4]. In addition, the characterization of hydrogen interaction with supported nickel nanoparticles, is not only important for the understanding of hydrogen storage using supported transition metals, but also due to its role on several chemical processes involving dissociative hydrogen adsorption, such as hydrogenation, hydrogenolysis reactions and many other chemical processes [11,12].

DFT is an important tool for the atomic level understanding of nickel-hydrogen interaction. Several studies have reported DFT calculations of hydrogen adsorption energyon Ni(1 1 1) for surface and sub-surface sites. Greenley et al. [11] reported a phase diagram considering the surface and sub-surface sites at different hydrogen coverages. They found that due to the high pressures required, it would be very difficult to produce sub-surface hydrogen on Ni(1 1 1). However, when considering strain on the surface, the formation of sub-surface hydrogen at lower pressures was observed, opening the possibility for subsurface hydrogen formation in strained Ni crystals (that could be generated by surface defects) under conditions of catalytic hydrogenation or hydrogen storage [13]. It is important to note that the kind of strain considered in that study was bulk-induced strain, not the compressive strain characteristic of small nanoparticles.

Bin Liu et al. [14] studied by DFT calculations the effect of Ni nanoparticles geometry on H_2 dissociation over Ni(1 1 1) and Ni_{13}. They found that, because of the strong affinity between H_2 and the Ni surface, regardless of its configuration, H_2 dissociation barriers decrease in the following order $Ni_4 > Ni_{13} >$ and Ni(1 1 1).

DFT studies of graphene-supported clusters have shown that the deposition of metal clusters is thermodynamically favored, with binding energies of −0.87 eV for a Fe_{13} cluster supported on pristine graphene [15].

Lim [16] studied the influence of defective graphene as support of Fe and Al nanoparticles, obtaining relatively strong adsorption

* Corresponding author.
E-mail address: samaya@unsl.edu.ar (S. Amaya-Roncancio).

https://doi.org/10.1016/j.apsusc.2018.03.233
0169-4332/

energies on the monovacancy defect site of graphene of −6.98 eV and −3.84 eV for Fe_{13} and Al_{13}, respectively. In these systems, charge transfer has been observed from the bound nanoparticles to the graphene surface, with potential beneficial consequences in the catalytic behavior of metal/graphene surfaces. As far as we know, the Ni_{13}/graphene system has not been studied by DFT, as well as its interaction with hydrogen.

In this work, hydrogen adsorption on Ni(1 1 1), 13-atoms nickel cluster (Ni_{13}) and graphene-supported Ni_{13}, was studied by DFT calculations. The main objective was analyzing the interaction of hydrogen with isolated Ni_{13} and graphene supported Ni_{13}, with a special focus on H_2 dissociative adsorption. In addition, the role of pre-adsorbed hydrogen on the energetics of the mentioned processes was evaluated.

2. Computational methods

DFT calculations were performed using the Quantum Espresso package [17]. The generalized gradient approximation (GGA) functional Perdew–Burke–Ernzerhof (PBE) was used [18]. Ultrasoft pseudopotentials with scalar relativistic correction generated by Rappe-Rabe-Kaxiras-Joannopoulos method (RRKJUS) were employed to describe the electron–ion interaction [19]. The chosen energy cutoff was 40 Ry and the threshold for self-consistency of 1×10^{-5} eV. Brillouin zone integration was approximated using the Monkhorst–Pack scheme with $3 \times 3 \times 1$ k-point sampling [20]. The calculated lattice parameter of the Ni bulk is 3.50 Å which is in good agreement with the experimental value of 3.52 Å [21]. The calculated total magnetization was of 0.69 μ_B/Ni-atom, which is consistent with previously reported values of 0.69 μ_B/Ni [11]. To model the Ni surface, calculations were performed in a $p(2 \times 2)$ supercell with a five-metal-layer slab model. Here, the first two layers were fixed at the bulk position and the other three layers were free to relax. The vacuum space between the slabs was set with a thickness of 10 Å. Graphene calculations were performed with a (5×5) supercell with a 20 Å vacuum. Ni_{13} was modeled using a Mackay icosahedrons shape [22]. All atoms of the Ni_{13}/graphene model were free to relax in order to find the minimum energy position of all the atoms involved [15,22]. The geometry relaxation was performed using BFGS quasi-Newton algorithm until the forces on each atom were less than 10^{-5} eV/Å and the energy difference of consecutive steps was less than 10^{-5} eV. The study of the minimum energy paths was undertaken using the nudged elastic band method (NEB) and local minima were found through the conjugate gradient CG technique [20,23]. All the minima and the saddle point states were confirmed through full vibrational frequency analysis [24]. Dispersion corrections to take into account the long range interactions, as the van der Waals ones, were previously made. The results have shown that these interactions do not have a significant effect in the adsorption energy calculations neither in the adsorption H_2 pathways of the studied systems (less than 0.1 eV). All molecular and density plots were made with the XCrySDen package [25].

3. Results and discussion

Calculations of adsorption energies of atomic hydrogen on the preferential adsorption sites of the Ni(1 1 1) surface, isolated Ni_{13} and graphene supported nickel cluster (Ni_{13}/graphene) were performed. The adsorption energies, bond energies and interaction energies (E_{bind}) of the Ni(1 1 1), Ni_{13} and Ni_{13}/graphene systems are presented in Tables 1 and 2, and were calculated using the following equation:

$$E_{bind} = E_{sys} - (E_{surf} + E_{mol}), \quad (1)$$

Table 1
Adsorption sites, adsorption energies and bond distances of hydrogen on Ni(1 1 1).

Site	E_{ads} (eV)	H-distance (Å)
fcc	−3.81	0.72
hcp	−3.81	0.74
1ML of H Coverage	−2.42	0.83 (On fcc) and 0.68 (Under hcp)
Under-Top (1st sub-layer)	−3.25	1.66 (Under Surface)
Octahedral (2st sub-layer)	−2.88	3.28 (Under Surface)

Table 2
Adsorption energy of hydrogen and co-adsorbed (20H*) hydrogen on Ni_{13} (isolated) and Ni_{13}/graphene.

System	E_{ads} (eV)	Distance (Å)
H on Ni_{13}	−3.78	0.93
20H on Ni_{13}	−2.46	0.92
H on (Ni_{13}/graphene)	−3.70	1.04
20H on (Ni_{13}/graphene)	−2.35	0.99

where E_{sys} is the total energy of H/Ni(1 1 1), H/Ni_{13} or Ni_{13}/graphene; E_{surf} the total energy of Ni(1 1 1), Ni_{13} or Ni_{13}/graphene; and E_{mol} the total energy of the adsorbed molecule in vacuum. The pseudo charge density difference $\Delta\eta$ was calculated using Eq. (2), as previously proposed by Gomez et al. [26]

$$\Delta\eta = \eta_{sys} - (\eta_{surf} + \eta_{mol}), \quad (2)$$

where η is the charge density; and the subscript *sys* refers to hydrogen adsorbed on Ni(1 1 1), Ni_{13} or Ni_{13}/graphene, *surf* refers to clean Ni(1 1 1), Ni_{13} or Ni_{13}/graphene and *mol* refers to the isolated hydrogen molecule.

4. Atomic hydrogen on Ni(1 1 1) surface

The adsorption sites and adsorption energy of atomic hydrogen on the Ni(1 1 1) surface were studied and are shown in Table 1 and Fig. 1. The calculations show the fcc and hcp sites are the preferential adsorption sites on the Ni(1 1 1) surface. The adsorption energy of the H atom, calculated with Eq. (1), was −3.81 eV for both sites. Similar bond distances from the surface were observed for fcc (0.74 Å) and hcp (0.72 Å), Table 1. In the subsurface, the Under Top and Octahedral sites were calculated with adsorption energies of −3.25 eV and −2.88 eV, respectively. The distances of the H atom under the surface were of 1.66 Å and 3.28 Å for Under Top and Octahedral sites, respectively (Table 1).

The results presented are in good agreement with the ones reported by Greeley and Mavrikakis [27], who reported adsorption energies of −2.89 eV and −2.88 eV for H atom adsorption on fcc and hcp sites respectively, and a H-surface distance of 0.90 Å in both sites. They also reported Under-Top and Octahedral sites energies of −1.92 eV and −2.11 eV respectively.

The adsorption energy of 1 ML coverage of H was calculated, resulting in −2.45 eV per hydrogen. Here, hydrogen adsorbs on fcc sites at 0.83 Å from the surface, and hcp at 0.68 Å under the surface (Fig. 1c, Table 1).

5. Atomic hydrogen on isolated Ni_{13} cluster

A Ni_{13} cluster was modeled from the structure previously reported by Lin et al. [22], where the authors presented the use of icosahedra as the minimum energy geometry for Ni and Pt clusters. Linn et al. [28], reported the same structure to investigate the effect of Pd substitution on the catalytic properties of Ni_{13} and its interaction with hydrogen.

After geometric relaxation, Ni-atom distances to the central Ni atom were 2.40 Å. The preferential adsorption site found for

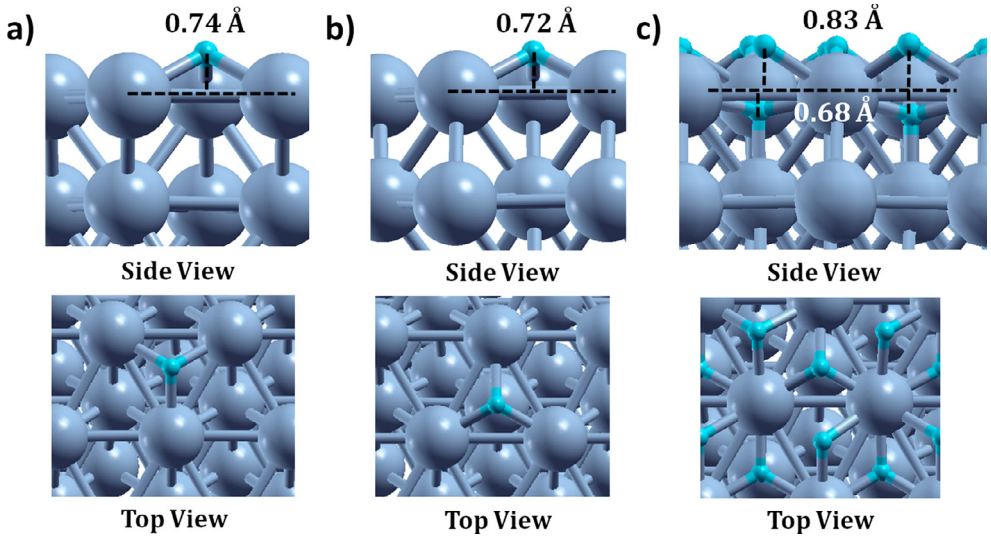

Fig. 1. Adsorption sites of hydrogen on Ni(1 1 1), (a) fcc site, (b) hcp site and (c) 1ML of H coverage. Gray: Ni; Cyan: Hydrogen.

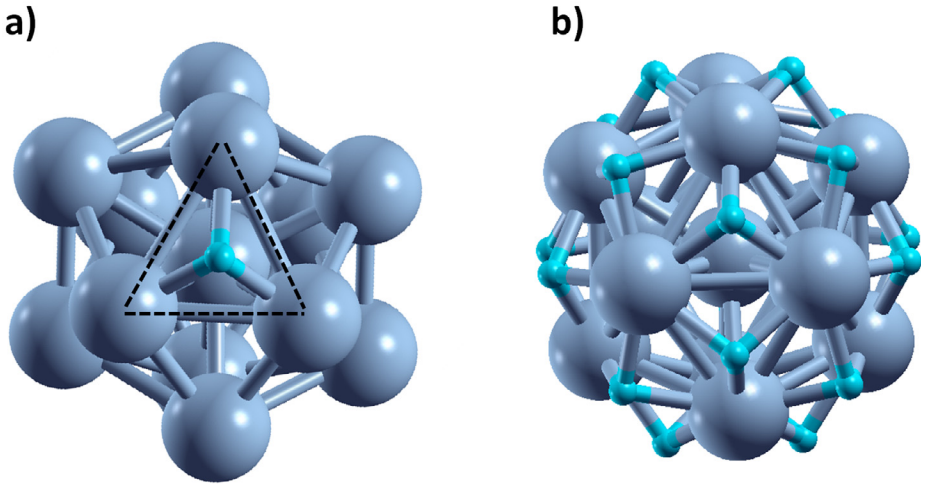

Fig. 2. Atomic hydrogen adsorption on, (a) threefold site of isolated Ni_{13}, (b) coadsorption of 20H atoms on threefold sites of isolated Ni_{13}.

hydrogen on Ni_{13} was the threefold site (Fig. 2a). The calculated adsorption energy for the H atom was −4.60 eV and the distance to the surface was 0.93 Å (Table 2). The presented results show consistency with Linn et al. [28], who reported an adsorption energy for atomic hydrogen of −4.14 eV and the threefold site as the preferential site. In addition, Liu et al. [14] also presented the threefold site as the preferential site of H on Ni_{13} with an adsorption energy of −3.12 eV.

The H-Ni_{13} interaction shows to be 0.36 eV more stable than the one calculated for the Ni(1 1 1) surface.

To study the effect of hydrogen co-adsorption on H-Ni_{13} interaction, 20 co-adsorbed H atoms were relaxed on Ni_{13} threefold sites (Fig. 2b). The 20H atoms co-adsorbed modify the adsorption energy from −3.78 eV to −2.50 eV per hydrogen, with respect to the single H adsorption. The H-Ni_{13} distance calculated for the 20 co-adsorbed H was 0.92 Å (Table 2). The results show that at high H coverages, the of hydrogen adsorption energy on Ni_{13} decreases.

6. Ni_{13} on graphene

After geometric relaxation, no remarkable modification of the graphene surface or Ni_{13} was observed. A Ni_{13}-graphene distance of 2.00 Å was calculated, with a binding energy, calculated by Eq. (1), of −1.76 eV. This value is in accordance with the binding energy of −0.96 eV for a Ni atom on graphene reported by Johll and Kang [29]. Considering 20H co-adsorption on Ni_{13}, the Ni_{13}-graphene interaction calculated by Eq. (1) was −1.73 eV, and the distance 2.11 Å (Fig. 3c).

Covalent interaction in metal-cluster/graphene systems have been previously reported with an interaction behavior consistent with the present work. Xin Liu et al. [15], Ken-Huang Lin et al. [30] and Wu et al. [31] reported values for cluster-graphene interaction energies of −0.87 eV, −1.99 eV and −1.18 eV for clusters of Fe_{13}, Pt_7 and Pt_4, respectively.

After atomic hydrogen is adsorbed on the graphene-supported Ni_{13}, the general structures of Ni_{13} or graphene were not substantially modified. The adsorption energy of a H atom on Ni_{13} was calculated as −3.70 eV, and the calculated distance from the threefold site plane to the hydrogen was 1.04 Å (Table 2, Fig. 3b).

The comparison between the adsorption energy of a H atom on isolated Ni_{13} and the one supported on graphene, shows that the H adsorption energy slightly decreases in 0.08 eV in the latter system. In the Ni_{13}/graphene system with 20 co-adsorbed H,

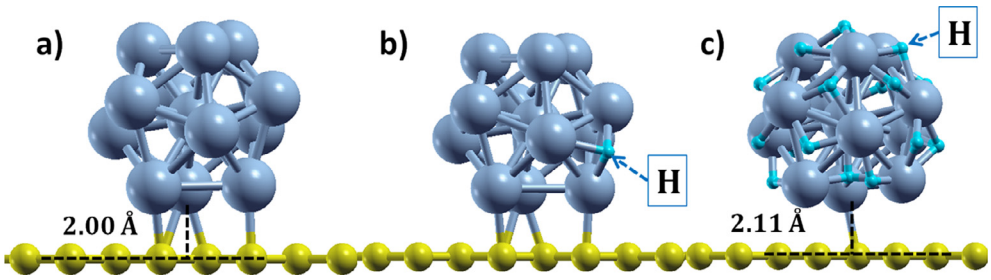

Fig. 3. Ni_{13} on graphene, (a) clean Ni_{13}/graphene, (b) Ni_{13}/graphene with a hydrogen atom chemisorbed, (c) Ni_{13}/graphene with 20 hydrogen atoms co-adsorbed.

the calculated bond energy per hydrogen was −2.35 eV, the Ni_{13}/graphene distance increased in 0.11 Å, and the H-adsorption site distances decreased to 0.99 Å (Table 2, Fig. 3c).

Comparing the effect of the 20H co-adsorbed on isolated Ni_{13} and graphene supported 20H/Ni_{13}, the adsorption energy decreases in 0.11 eV in the latter case.

In 20H on Ni_{13}/graphene the adsorption energy was 0.07 eV less stable compared with the calculated for 1 ML of H coverage on Ni(1 1 1) (Table 1, Table 2).

The pseudo charge density difference calculated with Eq. (2) (Fig. 4a), shows for the case of graphene-supported Ni_{13}; that the accumulation lobes (red) are mainly distributed around the Ni_{13}-graphene interface.

The present results are consistent with Liu et al. [15], who found a bond energy for the Fe_{13}/graphene system of −0.87 eV, a distance of 2.15 Å and reported a similar behavior of charge density with the same cluster geometry.

When an H atom is chemisorbed on the Ni_{13}/graphene system, the charge density shows accumulation around it due to Ni_{13} donation. Anadditional contribution from the graphene surface is also observed (Fig. 4b).

In the case of 20H co-adsorbed on the Ni_{13}/graphene, the accumulation lobes are mainly located on the H-Ni_{13} bond. Due to the presence of chemisorbed hydrogen atoms and their electron withdrawal effect, the accumulation of charge density around the Ni_{13}-graphene interface decreases in 0.03 eV respect to Ni_{13}-graphene (Table 2, Fig. 4b and c).

7. Dissociative adsorption of H_2 on Ni(1 1 1), Ni_{13} and Ni_{13}/graphene

For the calculation of dissociative H_2 adsorption on a Ni(1 1 1) surface, the initial state corresponded to a H_2 molecule at a distance of 2.30 Å from the surface, and the final state to two H atoms adsorbed on adjacent fcc and hcp surface sites (Fig. 5a).

At 1ML of H coverage, a similar initial state was set and the final state was considered with the two H atoms co-adsorbed in fcc and hcp sites, taking into account the positions previously calculated (Fig. 5b).

The adsorption of H_2 on Ni(1 1 1) is a non-activated process, the energy found for dissociative H_2 adsorption on Ni(1 1 1) was 2x

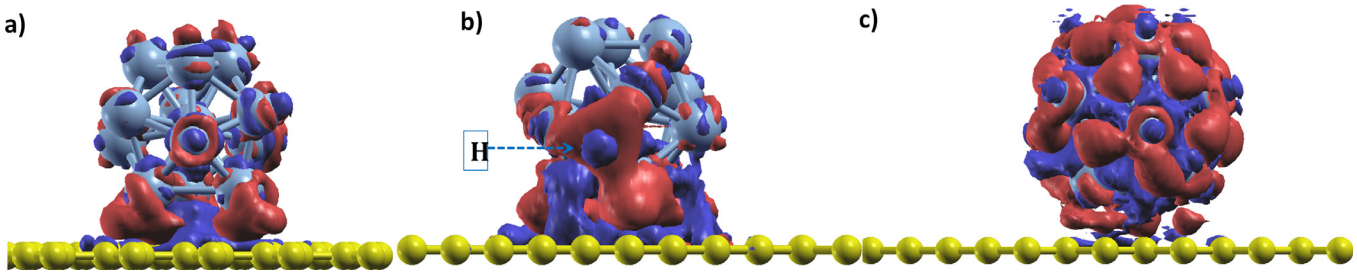

Fig. 4. Pseudo charge density difference of: (a) Ni_{13} supported on graphene with respect to isolated Ni_{13} and graphene, (b) adsorbed H on Ni_{13}/graphene with respect to isolated H, Ni_{13} and grapheme, and (c) 20H on Ni_{13}/graphene with respect to isolated 20H, isolated Ni_{13} and graphene at the same positions. Red lobes indicate accumulation and blue lobes depletion. Isosurface value 0.001 eV/Å^3. (For interpretation of the references to colour in this figure legend, the reader is referred to the web version of this article.)

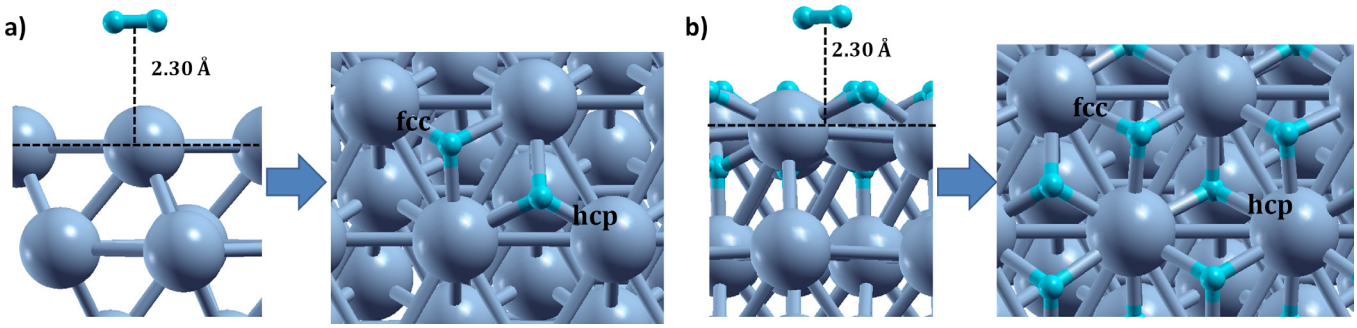

Fig. 5. Initial and Final state of H_2 adsorption on: (a) clean Ni(1 1 1), (b) Ni(1 1 1) pre-covered with 1-ML of H.

Table 3
Activation energies of $(H_2)_g$ adsorption on Ni(1 1 1), Ni_{13} (isolated) and Ni_{13}/graphene system. E_{act} represents activation energy, (*) indicates adsorption sites or adsorbed species.

System	Reaction	E_{act} (eV)	ΔE (eV)
Ni(1 1 1)	$(H_2)_g + 2^* \leftrightarrow 2H^*$	–	−0.76
1ML-H^*/Ni(1 1 1)	$(H_2)_g + 2^* + 6H^* \leftrightarrow 8H^*$	–	−0.94
Ni_{13}-isolated	$(H_2)_g + 2^* \leftrightarrow 2H^*$	–	−1.06
$(18H^*)$ Ni_{13}-isolated	$(H_2)_g + 2^* + 18H^*_* \leftrightarrow 20H^*$	–	−1.44
Ni_{13}/graphene	$(H_2)_g + 2^* \leftrightarrow 2H^*$	0.10	−1.04
$(18H^*)$ Ni_{13}/graphene	$(H_2)_g + 2^* + (18H^*) \leftrightarrow 20H^*$	0.04	−1.12

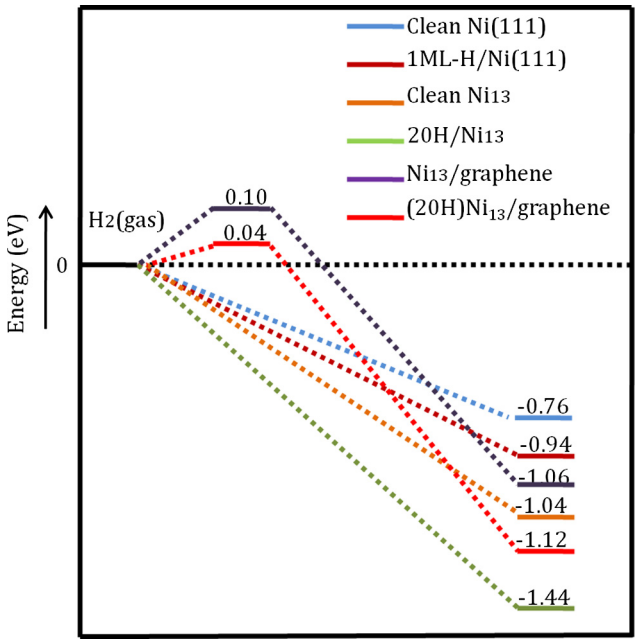

Fig. 6. Energy profiles of H_2 dissociation on Ni(1 1 1), Ni_{13}, and graphene-supported Ni_{13}. The effect of pre-adsorbed H is also shown.

(−0.38) = −0.76 eV (Table 3 and Fig. 6). These energy values are in good agreement with the results of Remediakis et al. [32], who reported an adsorption energy for $\frac{1}{2}$ (H_2) on Ni(1 1 1) of −0.39 eV, which corresponds to 2x(−0.39) = −0.78 eV. Besides, Shirazi et al. [12], reported the dissociative H_2 adsorption energy on Ni(1 1 1) as −0.75 eV.

For the adsorption of H_2 on Ni(1 1 1) with 1 ML of H coverage the reaction remains non activated. The calculated dissociative adsorption of H_2 was 2x(−0.47) = −0.94 eV (Table 3, Fig. 6).

Regarding isolated Ni_{13} and the 20H/Ni_{13}, the considered initial state was a H_2 molecule at a distance of 3.55 Å. That distance was chosen to consider as negligible the H_2-Ni_{13} interaction (Fig. 7a and b). The final state in Ni_{13} was the two H atoms adsorbed at 0.98 Å from the threefold site plane as shown in Fig. 7a. It was observed that H_2 dissociation is a non-activated process with an adsorption energy of 2x(−0.53 eV) = −1.06 eV (Table 3, Fig. 6). The present result is in accordance with Liu et al. [14], who reported the same H_2 adsorption on Ni_{13} with a backward barrier of 1.01 eV.

In the 20H on Ni_{13}, the final state showed the H atoms adsorbed at 0.92 Å from the threefold site plane. As for isolated Ni_{13}, the process is non-activated while the reverse barrier calculated was 1.44 eV (Table 3, Fig. 6).

In comparison with Ni(1 1 1), the final states of isolated Ni_{13} and 20H on Ni_{13} are 0.30 eV and 0.68 eV more stable respectively. Thus, we found that dissociative H_2 adsorption presents higher stabilization on Ni_{13} and 20H on Ni_{13}, compared with the same process on Ni(1 1 1) (Table 3 and Fig. 6).

In graphene supported Ni_{13}, a molecular hydrogen at 4.52 Å from the Ni_{13} was considered as the initial state (Fig. 8a). The transition state was reached at 2.24 Å and the final state was two H atoms adsorbed on adjacent threefold sites (Fig. 8b and c). The activation barrier calculated was 0.10 eV, with a backward barrier of 1.04 eV (Table 3 and Fig. 6).

In the Ni_{13}/graphene with 18H pre-adsorbed, the initial and final states were considered as in the previous case. The process was found to be slightly activated with 0.04 eV and the backward barrier calculated was 1.12 eV (Table 3, Figs. 6 and 8d–f).

We consider that the charge density depletion on the Ni_{13}/graphene, due to its accumulation around the Ni_{13}-graphene interface, makes H_2 adsorption electronically less favorable (Fig. 4a and b). The lack of charge density around the adsorption sites of supported Ni_{13} (effect of the depletion), would be responsible for the appearance of the activation barrier (Table 3 and Fig. 6). When H co-adsorption is considered, a redistribution of charge density is observed (Fig. 4c), decreasing the activation barrier generated in the phenomenon mentioned above. These results seem to be of great importance in the catalytic behavior of Ni clusters on graphene systems.

Hence, we found that H_2 dissociation on Ni_{13}/graphene maintains its exothermic character, and the presence of pre-adsorbed hydrogen reduces the activation barrier for the process and increases the stability of the final state.

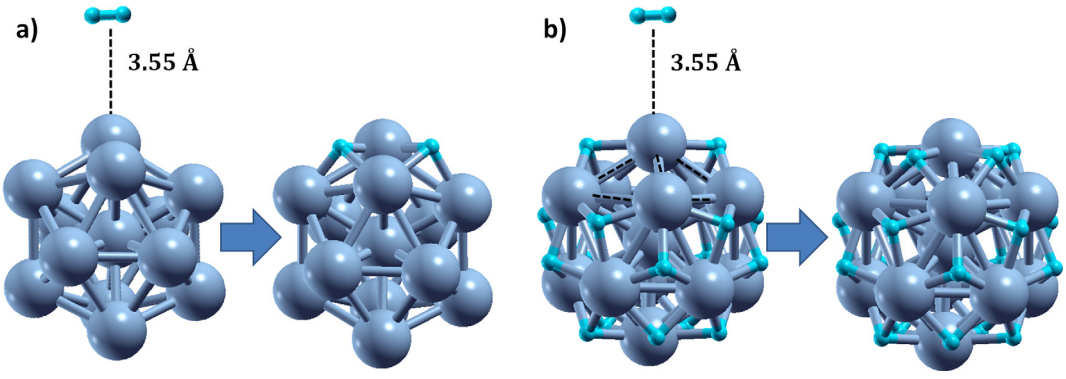

Fig. 7. Initial and Final state of H_2 adsorption on: (a) clean isolated Ni_{13} cluster, (b) isolated Ni_{13} cluster pre-covered with 18H.

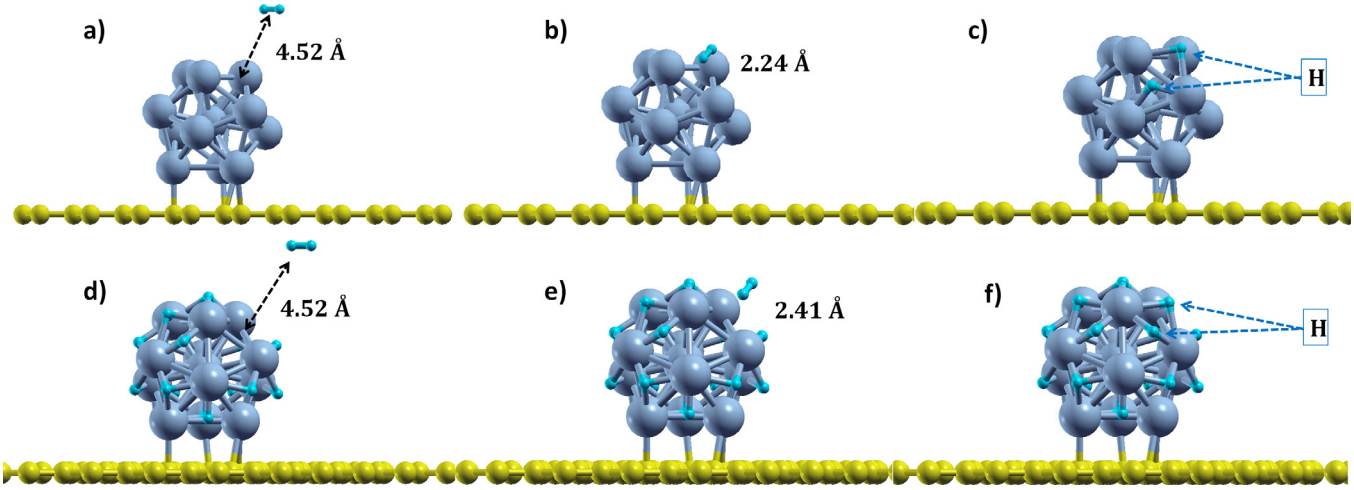

Fig. 8. H_2 adsorption on graphene-supported Ni_{13}: (a) initial state of H_2 on Ni_{13}/graphene, (b) transition state of H_2 on Ni_{13}/graphene, (c) final state of H_2 on Ni_{13}/graphene, (d) initial state of H_2 on Ni_{13}/graphene pre-covered with 18H, (e) transition state of H_2 on Ni_{13}/grapehene pre-covered with 18H, and (f) final state of H_2 on Ni_{13}/grapehene pre-covered with 18H.

8. Conclusions

The present work provides important insights on the interaction of hydrogen with Ni(1 1 1), isolated Ni_{13} and graphene supported Ni_{13}. The isolated Ni_{13} presents the highest energy of H atom adsorption (−3.78 eV) whereas H adsorption on graphene-supported Ni_{13} decreases to −3.70 eV, due to the electron transfer from the Ni_{13} cluster to the graphene surface. The dissociative adsorption of H_2 showed to be a non-activated process on Ni(1 1 1) and isolated Ni_{13}, while the process showed an activation barrier of 0.10 eV in graphene-supported Ni_{13}. The presence of pre-adsorbed H decreases the adsorption energy per H atom, stabilizes the final state in dissociative H_2 adsorption and reduces its activation barrier in graphene supported Ni_{13}.

Acknowledgment

The authors acknowledge the financial support of Argentinean Agencies of Science and Technology, FonCyT, CONICET and the National University of San Luis, which allowed the development of this work in special to PROIPRO 03-2516-UNSL.

References

[1] Tatiane da Silva Veras, Thiago Simonato Mozer, Danielle da Costa Rubim Messeder dos Santos, Aldara da Silva Cesar, Hydrogen: trends, production and characterization of the main process worldwide, Int. J. Hydrogen Energy 42 (2017) 2018–2033.
[2] Patrick Preuster, Alexander Alekseev, Peter Wasserscheid, Hydrogen storage technologies for future energy systems, Annu. Rev. Chem. Biomol. Eng. 8 (2017) 445–471.
[3] Michael G. Walter, Emily L. Warren, James R. McKone, Shannon W. Boettcher, Qixi Mi, Elizabeth A. Santori, Nathan S. Lewis, Solar water splitting cells, Chem. Rev. 110 (2010) 6446–6473.
[4] Jianwei Ren, Nicholas M. Musyoka, Henrietta W. Langmi, Mkhulu Mathe, Shijun Liao, Current research trends and perspectives on materials-based hydrogen storage solutions: a critical review, Int. J. Hydrogen Energy 42 (2017) 298–311.
[5] Hao Chen, Lifeng Wang, Jun Yang, Ralph T. Yang, Investigation on hydrogenation of metal−organic frameworks HKUST-1, MIL-53, and ZIF-8 by hydrogen spillover, J. Phys. Chem. C 117 (2013) 7565–7576.
[6] Froudakis, George M. Psofogiannakis, George, DFT study of hydrogen storage by spillover on graphite with oxygen surface groups, J. Am. Chem. Soc. 131 (2009) 15133–15135.
[7] Chen, Suresh K. Konda, Aicheng, Palladium based nanomaterials for enhanced hydrogen spillover and storage, Mater. Today 19 (2016) 100–108.
[8] Cheng-Si Tsao, Yun Liu, Haw-Yeu Chuang, Huan-Hsiung Tseng, Tsan-Yao Chen, Chien-Hung Chen, Yu. Ming-Sheng, Qixiu Li, r Angela Lueking, Sow-Hsin Chen, Hydrogen spillover effect of Pt-doped activated carbon studied by inelastic neutron scattering, J. Phys. Chem. Lett. 2 (2011) 2322–2325.
[9] Froudakis, George M. Psofogiannakis, E. George, DFT study of the hydrogen spillover mechanism on Pt-doped graphite, J. Phys. Chem. C 113 (2009) 14908–14915.
[10] Cristian I. Contescu, Craig M. Brown, Yun Liu, Vinay V. Bhat, Nidia C. Gallego, Detection of hydrogen spillover in palladium-modified activated carbon fibers during hydrogen adsorption, J. Phys. Chem. C 113 (2009) 5886–5890.
[11] Jeff Greeley, Manos Mavrikakis, A first-principles study of surface and subsurface H on and in Ni(111): diffusional properties and coverage-dependent behavior, Surf. Sci. 540 (2003) 215–229.
[12] Mahdi Shirazi, Annemie Bogaerts, Erik C. Neyts, DFT study of H-dissolution into the bulk of a crystalline Ni(111) surface: a chemical identifier for reaction kinetics, Phys. Chem. Chem. Phys. 19 (2017) 19150.
[13] J. Greenley, W.P. Krekelberg, M. Mavrikakis, Strain-induced formation of subsurface species in transition metals, Angew. Chem. Int. Ed. 43 (2004) 4296–4300.
[14] Bin Liu, Mark T. Lusk, James F. Ely, Influence of nickel catalyst geometry on the dissociation barriers of H_2 and CH_4: Ni_{13} versus Ni(111), J. Phys. Chem. C 113 (2009) 13715–13722.
[15] Xin Liu, Changgong Meng, Yu. Han, Unique reactivity of Fe nanoparticles–defective graphene composites toward NHx (x = 0, 1, 2, 3) adsorption: a first-principles study, Phys. Chem. Chem. Phys. 14 (2012) 15036–15045.
[16] Dong-Hee Lim, Ana Suarez Negreira, Jennifer Wilcox, DFT studies on the interaction of defective graphene-supported Fe and Al nanoparticles, J. Phys. Chem. C. 115 (2011) 8961–8970.
[17] P. Giannozzi et al., QUANTUM ESPRESSO: a modular and open-source software project for quantum simulations of materials, J. Phys. Condens. Matter 21 (2009) 1–9.
[18] M.C. Payne, M.P. Teter, C. Allan, T.A. Arias, J.D. Joannopoulos, Iterative minimization techniques for ab-initio total-energy calculations: molecular dynamics and conjugate gradients, Rev. Mod. Phys. 64 (1992) 1045–1097.
[19] Andrea Dal Corso H.pbe-rrkjus.UPF, Ni.pbe-nd-rrkjus.UPF, C.pbe-rrkjus. http://www.quantum-espresso.org. online 2014.
[20] G. Henkelman, B.P. Uberuaga, H. Jonsson, A, climbing image nudged elastic band method for finding saddle points and minimum energy paths, J. Chem. Phys. 113 (2000) 9901–9904.
[21] Charles Kittel, Introduction to Solid State Physics, eighth ed., John Wiley and Sons Inc, New York, 2005.
[22] Z.Z. Lin, X. Chen, C. Yin, H. Tang, Y.C. Hu, X.J. Ning, Theoretical prediction of the growth and surface structure of Pt and Ni nanoparticles, EPL 96 (2011) 66005.
[23] M.C. Payne et al., Iterative minimization techniques for ab-initio total-energy calculations: molecular dynamics and conjugate gradients, Rev. Mod. Phys. 64 (1992) 1045–1097.
[24] G.S. Otero, B. Pascucci, M.M. Branda, R. Miotto, P.G. Belelli, Evaluating the size of Fe nanoparticles for ammonia adsorption and dehydrogenation, Comput. Mater. Sci. 124 (2016) 220–227.
[25] A. Kokalj, Computer graphics and graphical user interfaces as tools in simulations of matter at the atomic scale, Comput. Mater. Sci. 28 (2003) 155–168.
[26] Elizabeth del V. Gómez, Sebastián Amaya-Roncancio, Lucía B. Avalle, Daniel H. Linares, M. Cecilia Gimenez, DFT study of adsorption and diffusion of atomic hydrogen on metal surfaces. 1–8, Appl. Surf. Sci. 420 (2017) 1–8.
[27] Mavrikakis, Jeff Greeley, Manos surface and subsurface hydrogen: adsorption properties on transition metals and near-surface alloys, J. Phys. Chem. B 109 (2005) 3460–3471.
[28] Linn Leppert, Rhett Kempe, Stephan Kummel, Hydrogen binding energies and electronic structure of Ni-Pd particles: a clue to their special catalytic properties, Phys. Chem. Chem. Phys. 17 (2015) 26140–26148.

[29] Kang, Harman Johll, Hway Chuan, Density functional theory study of Fe Co, and Ni adatoms and dimers adsorbed on graphene, Phys. Rev. B 79 (2009) 245416.
[30] Ken-Huang Lin, Chenghua Sun, Shin-Pon Ju, Sean C. Smith, Density functional theory study on adsorption of Pt nanoparticle on graphene, Int. J. Hydrogen Energy 38 (2013) 6283–6287.
[31] Hong-Yu Wu, Xiaofeng Fan, Jer-Lai Kuo, Wei-Qiao Deng, DFT Study of Hydrogen storage by spillover on graphene with boron substitution, J. Phys. Chem. C 115 (2011) 9241–9249.
[32] Ioannis N. Remediakis, Frank Abild-Pedersen, Jens K. Nørskov, DFT study of formaldehyde and methanol synthesis from CO and H_2 on Ni(111), J. Phys. Chem. B 108 (2004) 14535–14540.